Investigation of terahertz pulse generation in semiconductors pumped at long infrared wavelengths

Nelson M. Mbithi,[1,2] György Tóth,[1] Zoltán Tibai,[1] Imene Benabdelghani,[1,2] Luis Nasi,[1,2] Gergő Krizsán,[1,2] János Hebling,[1,2,3] Gyula Polónyi,[2,3,*]

[1]*Institute of Physics, University of Pécs, Ifjúság ú. 6, 7624 Pécs, Hungary*
[2]*Szentágothai Research Centre, University of Pécs, Ifjúság ú. 20, Pécs 7624, Hungary*
[3]*ELKH-PTE High-Field Terahertz Research Group, Ifjúság ú. 6, 7624 Pécs, Hungary*
*polonyi@fizika.ttk.pte.hu

Abstract: We present designs of semiconductor contact grating high energy terahertz pulse sources pumped by femtosecond pulses in the 1 to 5 μm wavelength range. Nearly wavelength-independent diffraction efficiencies as high as 69% and 75% in the ±1st diffraction orders in the transverse electric field polarization state were predicted in GaAs and GaP, respectively, based on rectangular grating. Numerical simulations – which contains, first to our knowledge, both the effect of nonlinear refractive index and free carrier absorption – were performed to investigate the possible advantage of using longer pumping wavelengths to suppress the 2- to 7-photon absorption. Conversion efficiency larger than 1.0% is predicted for both crystals. We also recognized that the nonlinear refraction index and the wavelength dependent OPA efficiency can significantly reduce the overall terahertz generation efficiency, thus optimum pump wavelengths exist for the highest conversion efficiency, which are 2 and 3 μm for GaP and GaAs, respectively.

1. Introduction

Recently, there has been a surge in developing highly efficient, scalable, and compact THz sources for example for biological [1], and medical research [2], or particle acceleration [3]. Among various approaches, THz generation by optical rectification (OR) provides an effective and tabletop solution for THz pulses flexibly tailored to the mentioned needs. At first, a semiconductor material was used in collinear geometry (i.e., ZnTe, pumped at 800 nm) with relatively low THz pulse energy and conversion efficiency [4, 5]. Although, $LiNbO_3$ has an almost 2.5 times bigger nonlinear optical coefficient than ZnTe, for a long time the lack of phase matching made it impossible to use it in the same arrangement. Twenty years ago, tilted pulse front pumping (TPFP) was invented to achieve phase matching in it at 810 nm [6], enabling the achievement of μJ-level pulse energies and beyond. Later, TPFP was applied to ZnTe as well, but the efficiency was highly limited due to two-photon absorption (2PA). The significance of the restraining effect of 2PA was clearly shown in [7], where both ZnTe and GaP were pumped at 1 μm wavelength. Although the nonlinear coefficient is more than two times less in GaP than in ZnTe, but at this wavelength the dominant multiphoton absorption order is 3PA for GaP and 2PA for ZnTe, resulting in a 3-times higher conversion efficiency for GaP. At the first efficient use of TPFP in semiconductors, the pumping wavelength was long enough to eliminate 2PA in GaAs and led to a conversion efficiency of 3.5×10^{-3} [8]. With the elimination of even the 3PA in ZnTe by using longer pump wavelength, as high as 0.7%

conversion efficiency has been reported [9]. This observed trend of increasing efficiency with longer pump wavelength raises the question of the existence of a practical limit where the costs of generating longer pump wavelengths are not in line with the reasonable yield in conversion efficiency. However, as far as we know, no one has ever investigated this argument yet.

The contact grating (CG) based on TPFP setup was proposed to achieve a collinear THz generation scheme with which the extractable THz energy became scalable with the crystal size and the pump beam [10] . The CG technique has been explored in $LiNbO_3$ [11] with relatively low efficiency. Then, it has been successfully designed [12]and implemented to ZnTe, where a conversion efficiency of 0.3% have been reported [13]. Since it is hard to grow single domain crystals from ZnTe, and the grown crystals often suffer from microbubbles which decrease the conversion efficiency [13], GaP and GaAs show promising alternatives as they are easier to grow and less expensive materials.

In this paper, we present design details of GaP and GaAs contact grating THz sources in the infrared wavelength range of 1-5 μm. A set of parameters that yield maximum diffraction efficiency are given. In addition, numerical calculations of THz pulse generation in GaP and GaAs in the broad infrared wavelength range are presented. Furthermore, first to our knowledge, the optimum pumping wavelength was also determined numerically, where the effect of the nonlinear refraction index and the wavelength dependence of the pumping OPA efficiency were also considered to give practical guidance for designing highly efficient THz pulse sources.

2. Models and approaches

2.1 Description of CG and determination of diffraction efficiencies

The contact grating (CG) scheme relies on a grating structure formed on the entrance surface of the semiconductor nonlinear crystal for tilting the pulse front [10]. As shown in Fig. 1(a), the pump beam is incident normally then diffracted at the grating surface. The diffraction angle ($\pm\beta$) is determined by the n_p (phase) index of the GaP/GaAs at the pump wavelength, and by the d grating groove spacing according to the grating equation given by Eq.(1) [12]

$$n_p \sin(\beta) = \pm \lambda_p / d \tag{1}$$

where λ_p is the pump wavelength.

In the two diffracted beams, the intensity fronts are tilted. It is clear that at normal incidence, the γ pulse front tilt (PFT) angle introduced by the diffraction equals to the β diffraction angle. Therefore, the groove spacing for a given wavelength was selected so that the angle appearing in Eq.(1) is equal to the PFT angle, which satisfy the velocity matching condition described by Eq. (2) [6]

$$\cos(\gamma) = \frac{n_g}{n_{THz}} \tag{2}$$

where, n_g is the group index, and n_{THz} is the THz refractive index, in the two symmetrical diffracted orders ($\pm$ 1st) the velocity matching condition is fulfilled. In this case, in the superposition of the two diffracted beams, the tilted pump pulse fronts are on each other and are parallel to the grating front. This superpositioned pump pulse front generates the THz pulse, which propagates collinearly with the original pump beam.

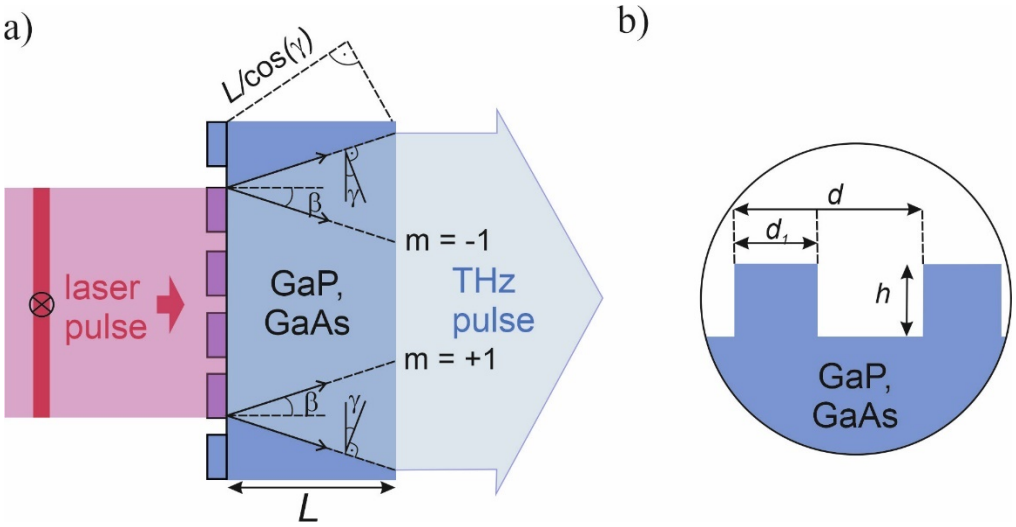

Fig. 1. Contact-grating scheme for GaP and GaAs (a), and (b) Cross-section of the structure; d – groove spacing, d_1 – linewidth and h – groove depth. The direction of the incident field is marked by ⊗, showing that it points out from the plane of the figure.

The optical, THz and group refractive indices were calculated from Sellmeier equations obtained from Ref. [14] and from Ref. [15] for GaAs and for GaP, respectively.

Fig. 1 (b) shows the cross-section of the structure. The parameters that define the diffraction efficiency are the h groove depth, and the f duty cycle (f=d_1/d). A set of these parameters, which give maximum diffraction efficiency, were determined from numerical calculations. The simulations were carried out using COMSOL Multiphysics software. The software is based on numerical solutions of partial differential equations utilizing finite element methods [16]. Transverse electric (TE) and transverse magnetic (TM) polarization states were studied for the rectangular grating profile (Fig. 1 (b)), where the TM polarization resulted in higher diffraction efficiencies. However, the TM polarization state was characterized by deep groove depths and low duty cycles, which is hard to fabricate, moreover, the effective nonlinear coefficient is 60% smaller typically compared to TE [17] resulting a significantly decreased THz generation efficiency. Hence, only the results for TE polarization will be considered and displayed in this article.

2.2. Simulation of THz generation

To investigate the optimal pump parameters for efficient THz pulse generation in GaP and GaAs, numerical calculations were done. The calculations were performed in the spectral domain by solving the one-dimensional wave equation with nonlinear polarization. The theoretical model used was based on Ref. [18] and took into account the following factors: pump pulse length variation with propagation distance due to material and angular dispersion, absorption in the THz frequency range due to complex dielectric function and cascade up- and down-conversion. In contrast to Ref. [18], which simulated THz pulse generation in lithium niobate, which is a large bandgap dielectric, the model used here considered the effects of free carriers generated in the smaller bandgap semiconductors by the high intensity optical field on the THz field. The instantaneous refractive index and absorption of the semiconductors at the THz range were calculated according to Eqs.(3) and (4), respectively.

$$n_{THz}(\Omega,z) = \Re e\left(\sqrt{\varepsilon_{r0}(\Omega) + \varepsilon_{fc}(\Omega,z)}\right) \quad (3)$$

$$\alpha(\Omega,z) = {}^{2\Omega}/_{c}\, \Im m\left(\sqrt{\varepsilon_{r0}(\Omega) + \varepsilon_{fc}(\Omega,z)}\right) \quad (4)$$

where $\varepsilon_{r0}(\Omega)$ is the dielectric permittivity of the semiconductor without free carriers, and $\varepsilon_{fc}(\Omega,z)$ is the permittivity attributed to free carriers [19]. It is given by Eq. (5)

$$\varepsilon_{fc}(\Omega,z) = -\frac{q^2}{\varepsilon_0 m_{eff}} \frac{N_{wa}(z)}{\Omega^2 + i\,\Omega/\tau_{sc}} \quad (5)$$

Here, q is the charge of the electron, ε_0 is the vacuum permittivity, m_{eff} is the effective mass of the electron, τ_{sc} is the electron scattering time, $N_{wa}(z)$ is the weighted average of the free carrier density at the z point in the crystal, which was determined according to Eqs. (6) and (7)

$$N_{wa}(z) = \frac{\int_{-\infty}^{\infty} A_{THz}^2(t,z) N_c(z,t)\mathrm{d}t}{\int_{-\infty}^{\infty} A_{THz}^2(t,z)\mathrm{d}t} \quad (6)$$

$$N_c(z,t) = \frac{\beta_n}{n h \nu_0} \int_{-\infty}^{t} I_{op}^n(t',z)\mathrm{d}t' \quad (7)$$

where β_n is the nth photon absorption coefficient, h is the Planck constant, ν_0 is the central pump frequency and $I_{op}(t,z)$ is the temporal intensity of the pump at the z point.

Pump wavelengths in the range of 1 to 5 μm were considered in the calculations. The lowest order effective MPA considered was 2PA and 3PA in GaAs and GaP, respectively. The MPA coefficients used in the calculations were obtained as follows; 2PA and 3PA coefficients of GaP were obtained from Ref. [20], and 2PA and 3PA coefficients of GaAs were obtained from Ref. [21] and Ref. [22], respectively. The coefficients corresponding to 4 to 6PA in GaAs and 4 to 7PA in GaP were estimated due to the absence of known coefficients for these materials in the wavelength ranges of interest. Sohn *et al*. had measured photon absorption coefficients up to the 11th order in GeSbS chalcogenide glass using the z-scan technique over a wavelength range of 1.1 μm to 5.5 μm [23]. It was revealed that the neighboring constants follow an exponentially decreasing scale, where the ratio between the neighboring values is nearly constant (see right column of Table 1). This is in accordance with the Keldysh photoionization model [24], which predicts an almost constant ratio as well. Based on this, we used the known constants of 2PA and 3PA to have the ratio (2PA/3PA$_{GaP}$: 95.2, 2PA/3PA$_{GaAs}$: 74.3) with which we estimated the missing values for higher orders when the intensity is in GW/cm^2 units. Table 1 summarizes the multiphoton absorption coefficients at various orders used in the simulations of THz pulse generation.

Table 1. **Multiphoton absorption (MPA) coefficients of GaP, GaAs and GeSbS glass**

MPA order	GaP	GaAs	GeSbS
2PA (cm/GW)	4 [20]	26 [21]	-
3PA ($\times 10^{-2}$cm^3/GW^2)	4.2 [20]	35 [22]	0.87 [23]
4PA ($\times 10^{-4}$ cm^5/GW^3)	4.4	47	1.1 [23]
5PA ($\times 10^{-6}$ cm^7/GW^4)	4.6	64	1.78 [23]
6PA ($\times 10^{-8}$ cm^9/GW^5)	4.8	86	2.38 [23]
7PA ($\times 10^{-10}$ cm^{11}/GW^6)	5.0	-	3.82 [23]

3. Results

3.1 Investigation of diffraction efficiency

Fig. 2(a) shows the plot of calculated diffraction efficiencies (DE) for the GaP CG with a groove spacing, $d = 1.7$ µm as a function of groove depth h, and duty cycle f, at 2.06 µm pump wavelength and a phase matching frequency of 2 THz. Diffraction efficiencies of more than 72% can be attained over the $h \approx 0.38$ to 0.46 µm groove depth-, and $f \approx 32$ to 43% duty cycle ranges, respectively, with a maximum diffraction efficiency of 74% at $h = 0.4$ µm and $f = 40\%$. A similar plot can be seen in Fig. 2(b) at 3.0 µm pump wavelength and 2 THz phase matching frequency with a groove spacing $d = 2.4$ µm. Diffraction efficiencies greater than 73% can be achieved over the $h \approx 0.59$ to 0.70 µm groove depth-, and $f \approx 40$ to 47% duty cycle ranges, respectively, with a maximum diffraction efficiency of 75% at $h = 0.65$ µm and $f = 45\%$.

Fig. 3(a) shows a plot of diffraction efficiencies for GaAs CG with a groove spacing, $d = 2.5$ µm versus groove depth h and duty cycle f, at 3.0 µm and a phase matching frequency of 2 THz. It can be evident in Fig. 3(a) that it is feasible to achieve diffraction efficiencies greater than 66% with $h \approx 0.45$ to 0.62 µm and $f \approx 30$ to 42%, with a maximum diffraction efficiency of 68% at $h = 0.55$ µm and $f = 37.5\%$. In addition, diffraction efficiencies greater than 67% were attained at 3.9 µm with optimal duty cycle and groove depth of $f \approx 30$ to 43% and $h \approx 0.63$ to 0.80µm, respectively (Fig. 3(b)), with a maximum diffraction efficiency of 69% at $h = 0.7$ µm and $f = 40\%$. Table 2 summarizes the numerical calculation results for the optimum diffraction efficiencies for GaAs and GaP at various selected wavelengths.

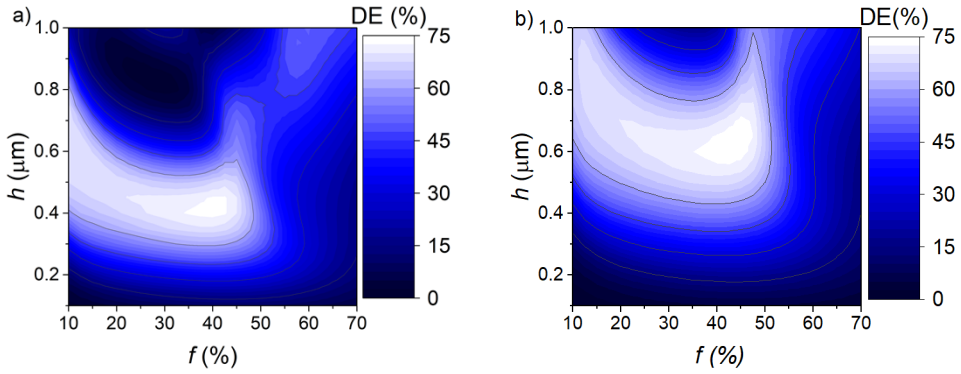

Fig. 2. CG based on GaP: Diffraction efficiency (DE) as a function of duty cycle *f* and groove depth *h* at 2 THz for (a) $\lambda_p = 2.06$ μm, groove spacing $d = 1.7$ μm, and (b) $\lambda_p = 3$ μm, groove spacing $d = 2.4$ μm, both for TE mode.

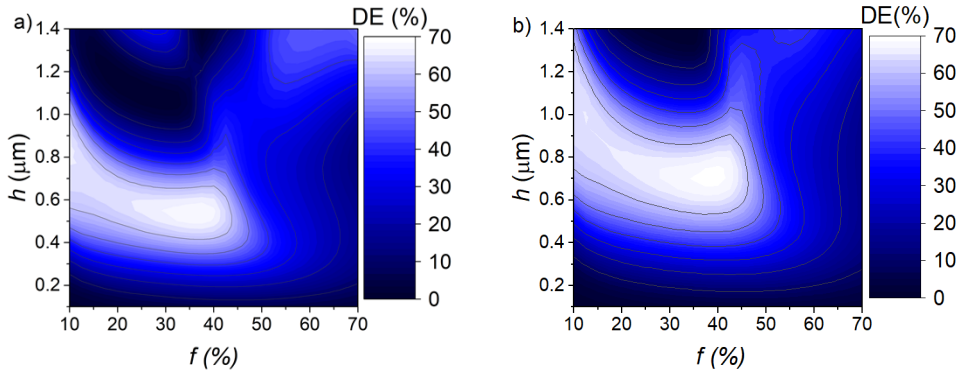

Fig. 3. CG based on GaAs: Diffraction efficiency (DE) as a function of duty cycle f and groove depth h, at 2 THz for (a) $\lambda_p = 3$ μm, groove spacing $d = 2.5$ μm and (b) $\lambda_p = 3.9$ μm, groove spacing $d = 3.1$ μm both for TE mode.

Table 2. Optimized parameters and calculated diffraction efficiencies at 2 THz for GaP and GaAs for TE polarization state

GaP						GaAs					
λ (μm)	$\gamma=\beta$ (°)	d (μm)	h (μm)	f (%)	DE (%)	λ (μm)	$\gamma=\beta$ (°)	d (μm)	h (μm)	f (%)	DE (%)
1.03	7.81	2.4	0.25	42.5	59	2.06	17.38	2.0	0.35	30	63
2.06	22.88	1.7	0.4	40	74	3.00	20.98	2.5	0.55	37.5	68
3.00	24.37	2.4	0.65	45	75	3.90	22.04	3.1	0.7	40	69

Table 2 shows the calculated diffraction efficiencies with optimized parameters at various wavelengths. The selection of the presented wavelengths was based on the simulations introduced later in this article. The middle ones correspond to the best THz generation efficiency, while the others are for somewhat shorter and longer wavelengths.According to Table 2, the diffraction efficiency increases with the wavelength in both GaP and GaAs. Moreover, GaP has better diffraction efficiencies at all wavelengths than GaAs. These behaviors can be attributed to the smaller Fresnel loss at lower index of refraction, and to the larger diffraction angles. The latter is favorable, since the larger the angle the lesser the number of the diffraction orders; thus, the diffracted beam is more concentrated in the lowest orders. It is worthy to note that using of antireflection coating could enhance the efficiency [25], but the investigation of this is beyond the scope of the present work.

3.2 Investigation of THz generation efficiency

Numerical simulations of terahertz generation in GaP and GaAs were performed at wavelengths corresponding to the suppression of various orders of multiphoton absorption to investigate the effect of the multiphoton absorption on the terahertz generation efficiency. In the case of GaP, the wavelengths correspond to the suppression of 2-, 3-, 4-, 5-, and 6PA, whereas in GaAs, the wavelengths correspond to suppression of 1-, 2-, 3-, 4-, and 5PA. The exact wavelength was chosen to be in the middle of the frequency range corresponding to the given order MPA.

3.2.1 Gallium phosphide

As an example, Fig. 4(a) depicts a plot of calculated THz generation efficiency (where the pump energy inside the crystal and the Fresnel loss at the output of the crystal were considered, but

the diffraction efficiency was not) as a function of pump pulse duration for various pump intensities at a pump wavelength of 1.98 μm, 4 mm crystal length and at 2 THz phase matching frequency. For the supposed wavelength, 5PA is the lowest order effective MPA process. At low pump intensity, the efficiency rises with intensity. Maximum efficiency of 0.72% was achieved at a pump intensity of 17.5 GWcm^{-2} and a pump pulse duration of 100 fs. At larger intensities, the efficiency decreased, and the optimal pump pulse duration shortened. This can be attributed to the increasing THz absorption of the fast-increasing density of free carriers with increasing pump intensity. A similar trend can be observed in Fig. 4(b) for a same type of plot of THz generation efficiency but at 2.9 μm pump wavelength, where 7PA is the lowest order MPA process. In this case, the optimal pump intensity increased to 27.5 GWcm^{-2}, and the efficiency increased to 1.14% for 125 fs pump pulse duration.

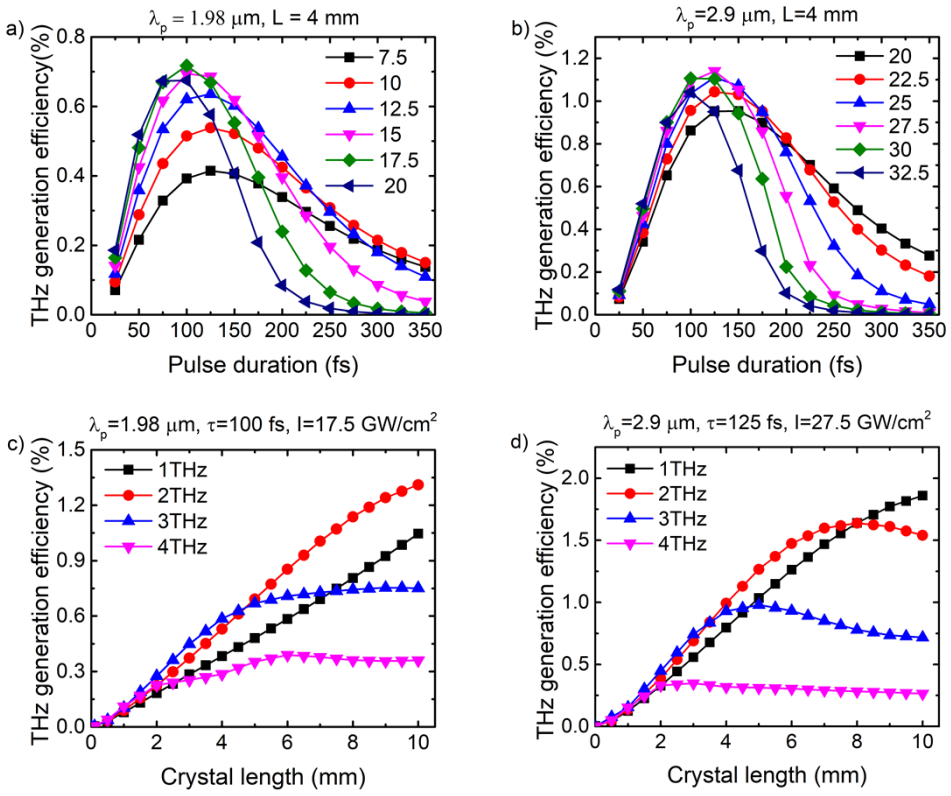

Fig. 4. THz generation simulation results for GaP. (a) and (b): efficiency of THz generation versus pulse duration at different pump intensities (in GW/cm^2) and at 1.98 μm and 2.9 μm pump wavelength, respectively, for 4 mm crystal length and for 2 THz velocity matching. (c) and (d): THz generation efficiency versus crystal length at 1.98 μm and 2.9 μm at 1, 2, 3 and 4 THz frequencies.

Fig. 4(c) depicts the efficiency dependence on the crystal length at a pump intensity of 17.5 GWcm^{-2}, a wavelength of 1.98 μm, and a duration of 100 fs at 1 THz, 2 THz, 3 THz, and 4 THz phase matching frequencies. The efficiency increases monotonically with crystal lengths at both 1 THz, 2 THz, and 3 THz, however, at 3 THz the increase is very modest for longer than 6 mm crystal length. At 4 THz, the efficiency increases with crystal length only up to 6 mm, followed by a slight decrease as the crystal length increases further. A similar behavior can be observed at 2.9 μm wavelength (Fig. 4(d)), with the difference that in this case, the saturation with the crystal length can be observed not only at 3 and 4 THz, but at 2 THz velocity

matching frequency, too. This observation can be attributed to absorption and dispersion, and to the larger group delay dispersion as well in the case of longer wavelength pumping, which increase with the THz phase matching frequency [26]. One reason for the plateau is the effect of back conversion which also grows with crystal thickness. This results in a shifted pump spectrum which spoils the phase matching.

3.2.2 Gallium arsenide

Fig. 5(a) depicts a plot of the calculated THz generation efficiency – in the same way as it was in the case with GaP – versus the pump pulse duration for various pump intensities at a pump wavelength of 2.06 μm, 4 mm crystal length, and 2 THz phase matching frequency. In this wavelength, 3PA is the lowest order effective MPA process. At low pump intensity, the efficiency increases with intensity. Maximum efficiency of 0.12% was achieved at 1.25 GWcm^{-2} pump intensity and a pulse duration of 100 fs. At higher intensities, the efficiency decreased, and the optimal pulse duration shortened, because of the free carrier absorption (FCA) in the same way as it was in GaP, except that at much smaller pump intensities. A similar trend can be observed in Fig. 5(b) for a plot of THz generation efficiency but at 3.85 μm pump wavelength, where 5PA is the lowest order MPA process. In this case the optimum pump intensity increased to 6 GWcm^{-2} and the efficiency increased to 0.9% at an optimum pulse duration of 125 fs.

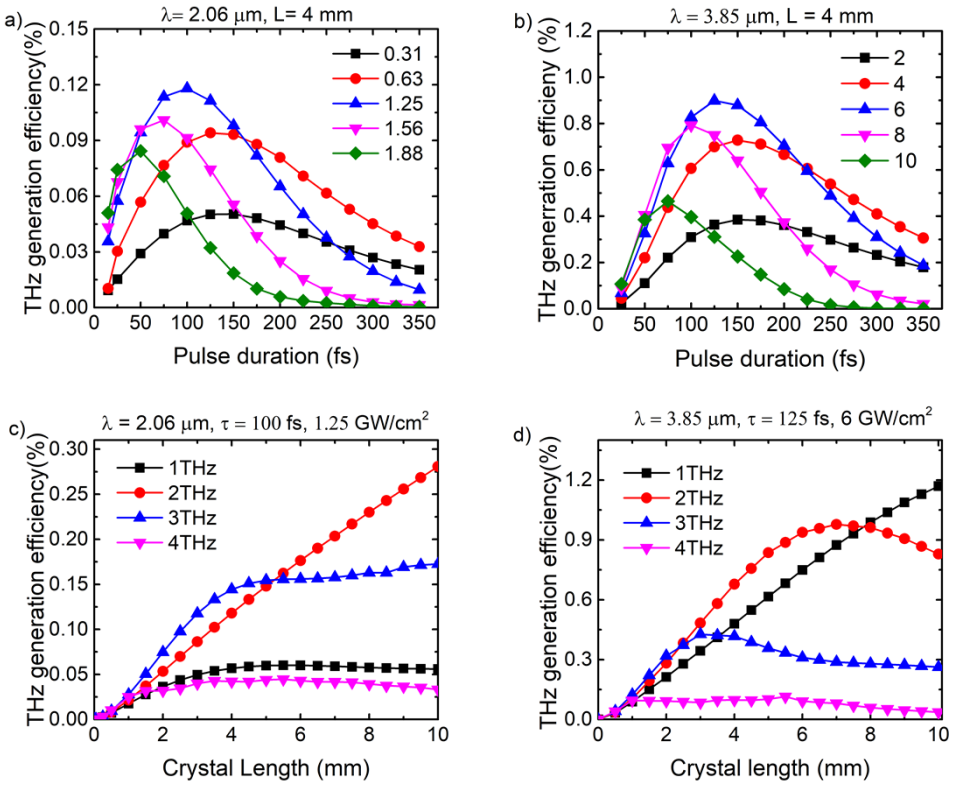

Fig. 5. THz generation simulation results for GaAs. (a) and (b) efficiency of THz generation versus pulse duration at different pump intensities (in GW/cm^2) and at 2.06 μm and 3.85 μm pump wavelength, respectively, for 4 mm crystal length and for 2 THz velocity matching, (c) and (d) THz generation efficiency versus crystal length at 2.06 μm and 3.85 μm at 1, 2, 3 and 4 THz frequencies.

Fig. 5(c) and (d) depict the efficiency dependence on crystal length at a pump intensity of 1.25 and 6 GWcm^{-2}, a wavelength of 2.06 and 3.85 µm, and at an optimum pulse duration of 100 and 125 fs, at 1 THz, 2 THz, 3 THz, and 4 THz phase matching frequencies. The monotonic increase with crystal length and the saturation of this increase at higher frequencies follow a similar trend to GaP, along with the movement of this saturation to the shorter thicknesses at longer wavelength. In these respects, the interpretation at GaP holds for GaAs as well. Comparing Fig. 4(c) with Fig. 5(c), the strong saturation of the THz generation efficiency at even short crystal length at 1 THz phase matching is evident on Fig. 5(c). We attribute this to the very strong effect of FCA at low THz frequency in the case of GaAs pumped at short wavelength, where 3PA with high coefficient is effective.

Despite the fact that GaAs has larger nonlinear coefficient, due to the smaller MPA, GaP outperforms it at short pump wavelengths. The smaller bandgap of GaAs compared to GaP results in disadvantageously larger MPA coefficients for a given order.

Although, throughout this work we focused on the conversion efficiencies, we would like to present simulated waveforms and spectrums as examples, too. Fig. 6(a) shows the THz field profiles for 2.06 µm and 3.85 µm pump wavelengths at optimum pump intensities of 1.25 and 6 GWcm^{-2}, and at an optimum pulse duration of 100 and 125 fs, respectively, for 4 mm thick crystal. At 2.06 µm pump wavelength, the electric field strength is approximately 16 kV/cm, whereas the electric field strength at 3.85 µm is about 90 kV/cm, which is 6 times higher. The reason for low field strength at 2.06 µm is due to strong 3PA and associated free carrier absorption, allowing the use of intensity 5 times less than at 3.85 µm. However, their corresponding spectrum of the THz field profiles at 2.06 µm and 3.85 µm pump wavelengths are comparable and extend to about 3THz, as shown in Fig. 6(b).

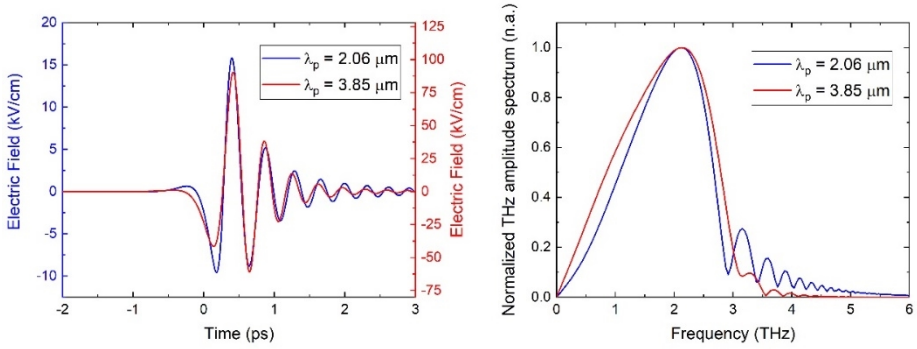

Fig. 6. (a) Simulation results for THz pulse field profiles for 4 mm thick GaAs for pump wavelengths 2.06 µm (blue) and 3.85 µm (red) and (b) The corresponding spectra, at 2 THz phase matching frequency.

4. Discussion

4.1 Effect of increasing pumping wavelength on the THz conversion efficiency

It has been predicted and demonstrated experimentally in many publications, that the elimination of low order MPA processes by using long pump wavelength can result in a significant increase of THz generation efficiency [8, 9, 27, 28], due to the possibility of using higher pump intensities without increasing the density of free carriers and their absorption in the THz range, (since the conversion efficiency is proportional to the pump intensity). However, according to our knowledge, there is no publication on the investigation of the possible practical

limit of useful pump wavelength. From the results of our series of numerical calculations, we can conclude that such a limit, and also an optimum pumping wavelength exists. The reasons for the finite optimum wavelength are: i) the yield from each eliminated multiphoton order is lessens with the order, ii) the cascade effect increases with the efficiency, and iii) most importantly, the efficiency of the optical parametric amplifier (OPA) supposed to be used for pumping the THz source decreases with wavelength owning to the Manley-Rowe relation.

To unveil the optimum pumping wavelength for the two different THz source materials, Fig. 7(a) depicts a plot of overall conversion efficiencies as a function of the MPA orders for GaAs and GaP, for crystal lengths of 4- and 7 mm. The overall conversion efficiency was obtained by multiplying the maximum THz generation efficiency at each corresponding wavelength of MPA order with the OPA efficiency (calculated using the Manley-Rowe relation, and supposing 50% conversion efficiency into the signal and idler beams together). In the case of GaAs, at 4 mm crystal length, the THz generation efficiency rises monotonically but with decreasing slope with MPA orders. At 7 mm crystal length, the efficiency increases steadily up to 4PA, then flattens, followed by a decrease with the order of MPA; thus, it is not favorable to go beyond the cut-off wavelength of 5PA (3850 nm). A similar behavior can be observed in both at 4 mm and 7 mm GaP, leading to an optimal pumping wavelength at about 2000 nm (above the cut-off wavelength of 4PA).

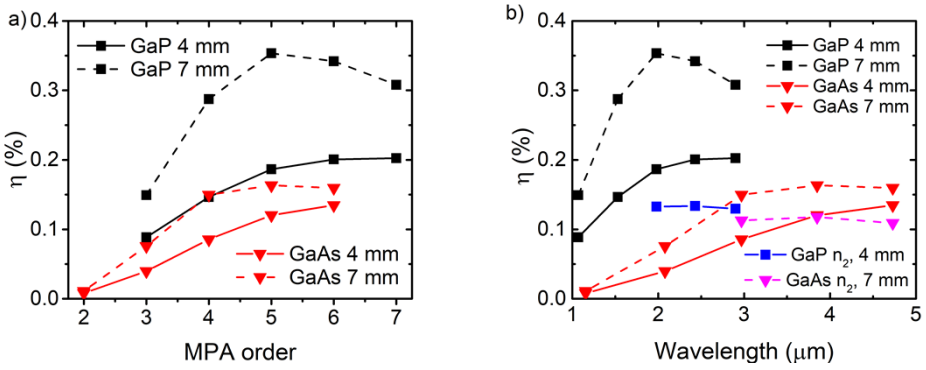

Fig. 7. Overall conversion efficiency(η) plotted against (a) MPA order and (b) wavelength for GaAs and GaP with the pumping OPA efficiency taken into account. Blue and magenta colors indicate results for GaP and GaAs, respectively when the effect of the nonlinear refraction was considered too.

4.2 Effect of nonlinear refraction on the THz conversion efficiency

In Ref. [18] (besides other processes) the effect of the nonlinear refraction on THz pulse generation in lithium niobate was investigated. We are unaware of such simulation of THz pulse generation in semiconductors, which considers this. Only the paper of Vodopyanov [27] mentions that it could possibly have some effect. We have performed numerical calculations to investigate the effect of nonlinear refraction through self-phase modulation on the generation efficiency as well. The model used for THz generation calculation was modified to take into account the nonlinear refractive index and its changes with the wavelength as stated in [29]. According to Fig. 7 (b), in the case of GaP, the efficiency reduced by about 30% for the 4 mm crystal length. In the instance of GaAs, the efficiency reduced by about 25% for 7 mm crystal length. Beside lowering the THz generation efficiency, self-phase modulation pushes the optimum pumping wavelength to shorter values.

5. Conclusion

We have demonstrated the basic designs of GaAs and GaP contact grating THz sources in order to develop efficient semiconductor THz sources for further upscaling of THz pulse energy and field strength by optical rectification of ultrashort laser pulses. The results reveal that rectangular contact grating profiles in the 1 to 5 μm infrared pump wavelength range can achieve diffraction efficiencies of 69% and 75% in GaAs and GaP, respectively. The optimal pumping conditions and phase matching frequency for ultrashort THz pulse generation via optical rectification in GaAs and GaP in the broad pump wavelength range were determined numerically. According to our calculations, a THz conversion efficiency of 0.9% and 1.14% can be achieved in GaAs and GaP, respectively. We realized an optimum pump pulse duration and phase matching frequency of 100-125 fs and 2 THz, respectively, for GaP and GaAs. We found that higher pump intensities can be used in GaP compared to GaAs. We also realized that pumping at longer wavelengths was better for higher THz generation efficiency due to the absence of strong low-order multiphoton absorptions. However, considering the decreasing efficiency of OPA pump source, there is a limit in pumping wavelength that is not prosperous to exceed, namely 3- and 2 μm (above the cut-off wavelengths of 4PA and 5PA) for GaAs and GaP, respectively. It was also found that the self-phase modulation due to nonlinear refractive index reduces the THz generation efficiency and pushes down the optimal pump wavelength. Therefore, in combination with novel infrared pump sources, like Ref. [30], GaAs and GaP THz sources can be good candidates for generating higher THz field strength for application in nonlinear THz spectroscopy and particle acceleration.

Acknowledgement. György Tóth would like to thank the support of the János Bolyai Research Scholarship of the Hungarian Academy of Science.
Funding. National Research, Development, and Innovation Office (2018-1.2.1-NKP-2018-00010, TKP2021-EGA-17), the Hungarian Scientific Research Fund (OTKA) (129134).

Disclosures. The authors declare no conflicts of interest.

Data availability. Data underlying the results presented in this paper are not publicly available at this time but may be obtained from the authors upon reasonable request.

References

1. M. H. Abufadda, A. Erdelyi, E. Pollak, P. S. Nugraha, J. Hebling, J. A. Fulop, and L. Molnar, "Terahertz pulses induce segment renewal via cell proliferation and differentiation overriding the endogenous regeneration program of the earthworm Eisenia andrei," Biomed. Opt. Express **12**, 1947-1961 (2021).
2. D. Nicoletti and A. Cavalleri, "Nonlinear light-matter interaction at terahertz frequencies," Adv. Opt. Photonics **8**, 401-464 (2016).
3. K. Zhong, W. Shi, D. Xu, P. Liu, Y. Wang, J. Mei, C. Yan, S. Fu, and J. Yao, "Optically pumped terahertz sources," Sci. China Technol. Sci. **60**, 1801-1818 (2017).
4. Q. Chen, M. Tani, Z. P. Jiang, and X. C. Zhang, "Electro-optic transceivers for terahertz-wave applications," J. Opt. Soc. Am. B **18**, 823-831 (2001).
5. A. Nahata, A. S. Weling, and T. F. Heinz, "A wideband coherent terahertz spectroscopy system using optical rectification and electro-optic sampling," Appl. Phys. Lett. **69**, 2321-2323 (1996).
6. J. Hebling, G. Almasi, I. Kozma, and J. Kuhl, "Velocity matching by pulse front tilting for large area THz-pulse generation," Opt. Express **10**, 1161-1166 (2002).
7. M. C. Hoffmann, K. L. Yeh, J. Hebling, and K. A. Nelson, "Efficient terahertz generation by optical rectification at 1035 nm," Opt. Express **15**, 11706-11713 (2007).
8. F. Blanchard, B. E. Schmidt, X. Ropagnol, N. Thiré, T. Ozaki, R. Morandotti, D. G. Cooke, and F. Légaré, "Terahertz pulse generation from bulk GaAs by a tilted-pulse-front excitation at 1.8 μm," Appl. Phys. Lett. **105**(2014).
9. G. Polonyi, B. Monoszlai, G. Gaumann, E. J. Rohwer, G. Andriukaitis, T. Balciunas, A. Pugzlys, A. Baltuska, T. Feurer, J. Hebling, and J. A. Fulop, "High-energy terahertz pulses from semiconductors pumped beyond the three-photon absorption edge," Opt. Express **24**, 23872-23882 (2016).

10. L. Pálfalvi, J. A. Fülöp, G. Almási, and J. Hebling, "Novel setups for extremely high power single-cycle terahertz pulse generation by optical rectification," Appl. Phys. Lett. **92**(2008).
11. M. Tsubouchi, K. Nagashima, F. Yoshida, Y. Ochi, and M. Maruyama, "Contact grating device with Fabry-Perot resonator for effective terahertz light generation," Opt. Lett. **39**, 5439-5442 (2014).
12. Z. Ollmann, J. A. Fulop, J. Hebling, and G. Almasi, "Design of a high-energy terahertz pulse source based on ZnTe contact grating," Opt. Commun. **315**, 159-163 (2014).
13. J. A. Fülöp, G. Polónyi, B. Monoszlai, G. Andriukaitis, T. Balciunas, A. Pugzlys, G. Arthur, A. Baltuska, and J. Hebling, "Highly efficient scalable monolithic semiconductor terahertz pulse source," Optica **3**, 1075-1078 (2016).
14. A. H. Kachare, W. G. Spitzer, and J. E. Fredrickson, "Refractive index of ion-implanted GaAs," J. Appl. Phys. **47**, 4209-4212 (1976).
15. J. Wei, J. M. Murray, J. O. Barnes, D. M. Krein, P. G. Schunemann, and S. Guha, "Temperature dependent Sellmeier equation for the refractive index of GaP," Opt. Mater. Express **8**(2018).
16. W. B. Zimmerman, *Multiphysics modeling with finite element methods* (World Scientific Publishing Company, 2006), Vol. 18.
17. G. Krizsán, Z. Tibai, G. Almási, G. Tóth, L. Pálfalvi, and J. Hebling, "New Generation Terahertz Pulse Sources Utilizing Volume Phase Holographic Gratings," in *High Intensity Lasers and High Field Phenomena*, (Optica Publishing Group, 2022), HF3B. 6.
18. K. Ravi, W. R. Huang, S. Carbajo, X. Wu, and F. Kartner, "Limitations to THz generation by optical rectification using tilted pulse fronts," Opt. Express **22**, 20239-20251 (2014).
19. P. Y. Yu and M. Cardona, "Vibrational properties of semiconductors, and electron-phonon interactions," in *Fundamentals of Semiconductors* (Springer, 2010), pp. 107-158.
20. V. Nathan, A. H. Guenther, and S. S. Mitra, "Review of Multiphoton Absorption in Crystalline Solids," J. Opt. Soc. Am. B: Opt. Phys. **2**, 294-316 (1985).
21. A. A. Said, M. Sheikbahae, D. J. Hagan, T. H. Wei, J. Wang, J. Young, and E. W. Vanstryland, "Determination of Bound-Electronic and Free-Carrier Nonlinearities in Znse, Gaas, Cdte, and Znte," J. Opt. Soc. Am. B: Opt. Phys. **9**, 405-414 (1992).
22. W. C. Hurlbut, Y. S. Lee, K. L. Vodopyanov, P. S. Kuo, and M. M. Fejer, "Multiphoton absorption and nonlinear refraction of GaAs in the mid-infrared," Opt. Lett. **32**, 668-670 (2007).
23. B. U. Sohn, M. Kang, J. W. Choi, A. M. Agarwal, K. Richardson, and D. T. H. Tan, "Observation of very high order multi-photon absorption in GeSbS chalcogenide glass," Apl. Photonics **4**(2019).
24. L. Keldysh, "Ionization in the field of a strong electromagnetic wave," J. Sov. Phys. JETP **20**, 1307-1314 (1965).
25. Z. Tibai, N. M. Mbithi, G. Almási, J. A. Fülöp, and J. Hebling, "Design of Semiconductor Contact Grating Terahertz Source with Enhanced Diffraction Efficiency," Crystals **12**(2022).
26. G. Polonyi, M. I. Mechler, J. Hebling, and J. A. Fulop, "Prospects of Semiconductor Terahertz Pulse Sources," IEEE J. Sel. Top. Quantum Electron. **23**, 1-8 (2017).
27. K. L. Vodopyanov, "Optical THz-wave generation with periodically-inverted GaAs," Laser Photonics Rev. **2**, 11-25 (2008).
28. J. Fülöp, L. Pálfalvi, G. Almási, and J. Hebling, "Design of high-energy terahertz sources based on optical rectification," Opt. express **18**, 12311-12327 (2010).
29. M. Sheik-Bahae, D. C. Hutchings, D. J. Hagan, and E. W. Van Stryland, "Dispersion of bound electron nonlinear refraction in solids," IEEE J. Quantum Electron. **27**, 1296-1309 (1991).
30. G. Andriukaitis, T. Balciunas, S. Alisauskas, A. Pugzlys, A. Baltuska, T. Popmintchev, M. C. Chen, M. M. Murnane, and H. C. Kapteyn, "90 GW peak power few-cycle mid-infrared pulses from an optical parametric amplifier," Opt. Lett. **36**, 2755-2757 (2011).